Heliyon 9 (2023) e22206

Contents lists available at ScienceDirect

Heliyon

journal homepage: www.cell.com/heliyon

Mix design process for sustainable self-compacting geopolymer concrete

M. Talha Ghafoor [a,b,*], Chikako Fujiyama [a]

[a] Graduate School of Urban Innovation, Department of Civil Engineering, Yokohama National University, Kanagawa, 240-8501, Japan
[b] Department of Civil Engineering, NFC Institute of Engineering and Fertilizer Research, Faisalabad, Pakistan

ARTICLE INFO

Keywords:
Compressive strength
Flow speed
Flow deformability
Self-compacting geopolymer concrete
Poisson's ratio
Young's modulus

ABSTRACT

Faster growth of infrastructure emphasizes the utilization of eco-friendly construction materials with a low carbon footprint. The objective of this experimental study is to propose a mix design methodology for self-compacting geopolymer concrete (SCGC) considering various influencing parameters recommended for self-compacting concrete (SCC) and geopolymer concrete (GPC). The experimental test results depict that SCGC had similar flow deformability with comparatively lesser flow speed compared to SCC. The increase in a sodium hydroxide (NaOH) molarity from 8 M to 16 M negatively affected the flow deformability as well as the flow speed of SCGC. The optimum compressive strength of 37 MPa was attained for SCGC having silica sand as fine aggregate, NaOH concentration of 16 M, fly ash to sand ratio (FA/S) of 0.75, and cured for 48 H at 80 °C. A mathematical equation is proposed to calculate Young's modulus of SCGC which is around 15 GPa. Young's modulus of SCGC was lesser than OPC concrete recommended by the ACI 318, however, Poisson's ratio of SCGC was found in the recommended range of OPC concrete. A flow chart is proposed for the mix design of SCGC with consideration of experimental test results in fresh and hardened stages.

1. Introduction

The concept of self-compacting concrete (SCC) was given in 1988 as a high-performance concrete having the advantages of self compatibility [1]. The higher volume of paste with a lesser amount of water in SCC plays a role in controlling segregation and bleeding [2]. The volume of water to powder ratio (Vw/Vp) and superplasticizer to powder ratio (Sp/P) are the main influencing factors that generally control the stress transformability in SCC [1,3]. SCC having lower yield stress, and moderate viscosity due to a presence of the limited amount of water is recommended as a high-performance concrete [4]. The coarse aggregate and fine aggregate content in SCC and SCM are usually fixed at 50 % of each of its packed densities, respectively [5]. The recommended volume of sand to mortar ratio and volume of coarse aggregate in SCC are about 45 % and 30 %, respectively [6]. Fine aggregate content also plays a role in controlling the fresh properties of SCC [7].

The application of SCC in the construction industry increases due to a wide range of advantages [8]. SCC requires double the amount of cement content compared to conventional concrete [6]. The construction industry is considered one of the major sources of carbon dioxide (CO_2) emissions throughout the world [9]. A sufficient amount of energy is emitted during the manufacturing of OPC as

* Corresponding author. Graduate School of Urban Innovation, Department of Civil Engineering, Yokohama National University, Kanagawa, 240-8501, Japan.
E-mail address: muhammadtalhaghafoor@gmail.com (M.T. Ghafoor).

https://doi.org/10.1016/j.heliyon.2023.e22206
Received 1 September 2023; Received in revised form 6 October 2023; Accepted 6 November 2023
Available online 10 November 2023

a result of energy-intensive processes [10]. CO_2 is the primary source of global warming and OPC generates about 5 %–7 % of CO_2 [11]. Researchers throughout the world have mainly focused on innovative binding materials that can be used in the replacement of conventional OPC [12].

The idea of Geopolymer concrete (GPC) named as an environmentally friendly concrete was given by Joseph Davidovits in 1978 [13]. No calcination process requirement in GPC provides greater support in controlling CO_2 production [14]. The binder for GPC includes any industrial waste (fly ash, slag) having a large amount of silica and alumina [15]. GPC not only reduces CO_2 emissions but also provides advantages to the utilization of by-product wastes [16]. Geopolymers reduced the greenhouse gas effect by 73 % and energy utilization by 43 % [14]. The lower workability due to the high viscosity of the alkaline solution is one of the biggest challenges in the practical implementation of GPC [17,18]. The slump of GPC was within a range of 5 mm–50 mm without the usage of any superplasticizer [19]. In another study, the reported slump for fly ash based GPC was found within the range of 45 mm–60 mm [20]. The cohesive paste of geopolymer demanded a higher content of superplasticizer in comparison to OPC paste to achieve comparable flow properties [21]. The workability of GPC is mainly affected by the amount of water, alkaline solution, geopolymer solid ratio, and alkaline activator to fly ash ratio [22]. The amount of fly ash also had an influence on the flow properties of geopolymer [23,24].

The parameters affecting the compressive strength of GPC include water to geopolymer solid ratio (W/GPS), sodium hydroxide (NaOH) molarity, alkaline activator to fly ash ratio (AA/FA), and curing temperature [15]. The curing temperature and alkaline activator solution both had an impact on the strength development of GPC, as both affect the geopolymerization mechanism [25]. The rate of exothermic reaction of GPC mainly depends on the curing temperature, therefore, curing temperature is the most important factor that affect the compressive strength of GPC [26,27]. The increase in curing temperature within the range of 50 °C to 80 °C increases the compressive strength of GPC by 100 % compared to ambient temperature [28]. The compressive strength of geopolymer mortar (GPM) was significantly affected with an increase in NaOH concentration [29,30]. The amount of fly ash had a positive impact on the compressive strength of GPC due to the formation of dense microstructure [31]. The compressive strength of GPC was increased from 31.25 % to 134.7 % with an increase in the quantity of fly ash. This is because of the dense microstructural formation as a result of an increase in fly ash content [31].

In terms of Young's modulus, the characteristics of geopolymer are discussed separately from compressive strength. Young's modulus of GPC is generally lower than conventional concrete due to the lesser Young's modulus of paste of geopolymer [32]. Young's modulus of GPC was less than 25 %–30 % compared to OPC concrete [33]. Young's modulus of SCC is also lesser than OPC concrete as a result of the presence of a lesser aggregate content [34].

Globally researchers try to develop a mix design for GPC with consideration of flow properties, as there are many limitations in the practical implementation of GPC including its relatively low workability. Self-compacting geopolymer concrete (SCGC) is an innovative idea to overcome low workability, however, limited studies are available [7,16,35–37]. Those studies mainly focus on achieving flow properties for GPC by increasing the percentage of superplasticizers without considering the importance of other constituents regarding flow properties. Furthermore, no study is available regarding the mix design of SCGC giving an idea about influencing parameters and boundary limits [38,39]. Consequently, it becomes imperative to propose a comprehensive mix design methodology for SCGC that incorporates the identification and characterization of various influencing parameters in order to widen its field application [40].

Here, the authors attempt to propose a different approach to realize self compacting geopolymer concrete (SCGC) based on the volume-based design method. As a first step, self-compacting geopolymer mortar (SCGM) was investigated with consideration of guidelines of SCM with the determination of fresh and hardened mechanical properties [18,36,41,42]. The authors are coming up with the next step which is to develop mix design for SCGC with consideration of volume. This means that the design principle of SCC is extended to GPC which always consists of high viscosity alkaline liquid. Then, as the last step, the target of this SCGC project was set as the achievement of compressive strength of more than 25 MPa by considering the impact of various parameters.

The volumetric proportion of constituents of SCGC in this study is summarized as shown in Fig. 1. The comparison of volumetric proportion along with the particle densities of solids and viscosities of liquid for SCC and SCGC (this study) is mentioned in Fig. 2, as well. The fresh mechanical properties (flow deformability, flow speed) of each SCGC mix were determined. The hardened mechanical properties including dry density, compressive strength, Young's modulus, and Poisson's ratio were also determined for SCGC. The

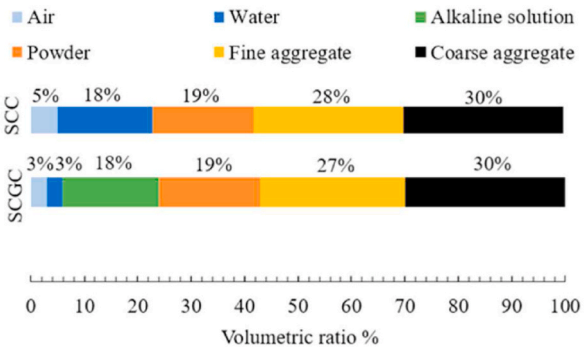

Fig. 1. Comparison of mix proportion of SCC and SCGC prototype (This study).

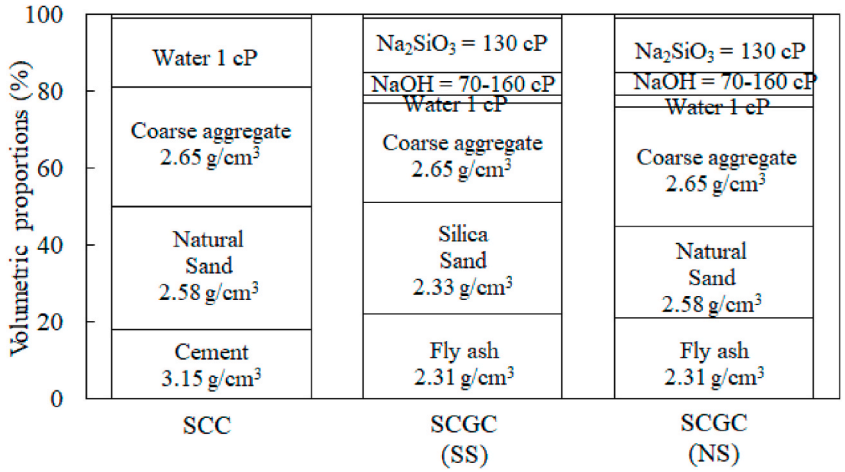

Fig. 2. Comparison of mix proportion of SCC and SCGC prototype along with particle densities of solid particles and viscosity of liquid.

stress–strain relationships for SCGC were also developed with the determination of axial and lateral strains using attached strain gauges. This study will particularly be beneficial to widen the field application of highly workable geopolymer concrete. Furthermore, due to the reduction in CO_2 as well as noise pollution, highly sustainable concrete could be attained in the form of SCGC having no need for external vibrations.

2. Experimental program

2.1. Materials

2.1.1. Fly ash

Fly ash was used as a binder for the preparation of self-compacting geopolymer concrete (SCGC). The chemical constituents of fly ash were determined using X-ray fluorescence (XRF), as mentioned in Table 1. The type of fly ash was found as class F based on the constituents of silica (SiO_2), alumina (Al_2O_3), iron oxide (Fe_2O_3), and calcium oxide (CaO) as per ASTM C618 [43]. The physical properties of fly ash are mentioned in Table 2.

2.1.2. Silica sand

Silica sand was used as a fine aggregate for the preparation of SCGC. The bulk density of silica sand was about 1446 kg/m^3. The particle size distribution curve of used silica sand is shown in Fig. 3. The chemical composition results of silica sand are mentioned in Table 3. Moreover, the physical properties of silica sand are mentioned in Table 4. The finer particle size of silica sand increases the filling ability which ultimately improves the microstructure of geopolymer [44].

2.1.3. Natural sand

The natural sand was also used as a fine aggregate in some SCGC mixes. The physical properties of natural sand are mentioned in Table 5. Moreover, the particle size distribution of used natural sand is shown in Fig. 4.

2.1.4. Coarse aggregate

The crushed stone was used as a coarse aggregate. The maximum size of coarse aggregate was 15 mm with average particles within a range of 5 mm–15 mm. The compacted bulk density of coarse aggregate was about 1600 kg/m^3. The physical properties of coarse aggregates are mentioned in Table 6.

2.1.5. Alkaline solution

Sodium hydroxide (NaOH) and sodium silicate (Na_2SiO_3) solution were used as alkaline activators. The NaOH molarity varied from 8 M to 16 M based on the variation of solids content [15,36]. The physical properties of the NaOH solution with a variation of NaOH molarity from 8 M to 16 M are mentioned in Table 7. The physical properties of the Na_2SiO_3 solution are mentioned in Table 8.

Table 1
Chemical composition results of fly ash using x ray fluorescence (XRF).

Constituents	SiO_2	Al_2O_3	Fe_2O_3	CaO	Na_2O	SO_3	K_2O	TiO_2	MgO	P_2O_5
%	57.24	31.07	3.27	1.86	0.76	0.27	1.32	0.97	2.04	0.78

Table 2
Physical properties of fly ash particles.

Description	Test value
Particle density	2.31 g/cm^3
Loss of Ignition	Less than 1.5 %

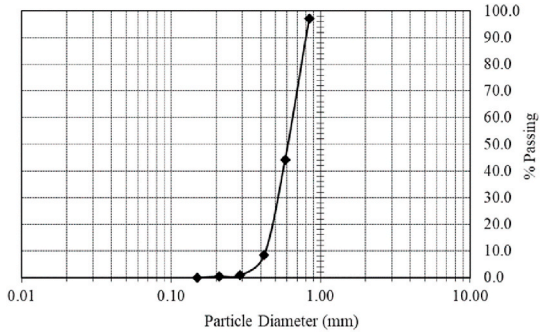

Fig. 3. Particle size distribution of silica sand.

Table 3
Chemical composition results of silica sand.

Constituents	Al_2O_3	SiO_2	CaO	Fe_2O_3	TiO_2	MgO
%	1.02	97.02	0.02	0.05	0.04	0.01

Table 4
Physical properties of silica sand.

Description	Test value
Main chemical constituents	SiO_2
Particle density	2.33 g/cm^3
Water absorption	0.5 % or less

Table 5
Physical properties of natural sand.

Description	Test value
Absolute dry density	2.52 g/cm^3
Surface dry density	2.58 g/cm^3
Water absorption	2.47 %
Coarse grain ratio	2.80

2.1.6. Superplasticizer

The polyaryl ether-based superplasticizer was used as high range water reducing admixture based on its significance in the alkaline environment of geopolymer [42]. The density of the superplasticizer was 1.01 g/cm^3 with a pH of 6.15.

2.2. Mix proportions

Seventeen (17) SCGC mixes were prepared to investigate the impact of various parameters on the fresh and hardened mechanical properties of SCGC. The sodium hydroxide (NaOH) concentration was varied from 8 M to 16 M and Na_2SiO_3/NaOH ratio was kept constant at 2.5 based on the recommendation of SCGM prototype [36]. The alkaline activator to fly ash ratio (AA/FA) was kept constant at 0.6 according to the recommendations of the previous study [18]. The volume of water to volume of powder ratio (Vw/Vp) varied from 0.87 % to 1.11 % and the volume of paste (Vpaste) varied within the range of 38 %–49 % according to the recommendations of normal SCC [1]. The volumetric proportions of SCGC mixes for one cubic meter (1 m^3) volume are presented in Table 9. Three (03) specimens of each mix were tested to take an average of compressive strength. Each mix was designated based on fly ash to sand ratio (FA/S), NaOH molarity, superplasticizer to powder ratio (Sp/P), coarse aggregate volume to solid volume (G/Glim), and

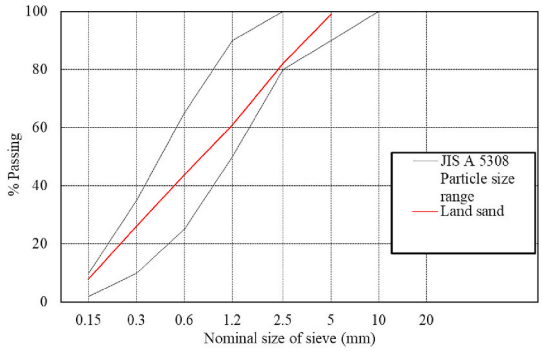

Fig. 4. Particle size distribution of natural sand.

Table 6
Physical properties of coarse aggregate.

Description	Test value
Absolute dry density	2.64 g/cm^3
Surface dry density	2.65 g/cm^3
Water absorption	0.55 %
Coarse grain ratio	6.50

Table 7
Physical properties of sodium hydroxide solution (NaOH).

NaOH solution	Mass (g/kg)	Density (g/cm^3)	Viscosity (cP)
8 M	262	1.26	70
10 M	314	1.31	–
12 M	361	1.37	110
14 M	404	1.40	–
16 M	444	1.44	160

Table 8
Physical properties of sodium silicate solution (Na_2SiO_3).

Appearance:	colorless to slightly colored liquid
SiO_2 (%)	29
Na_2O (%)	12
Density (g/cm^3)	1.47

type of sand. For example, the mix G-0.5-8-4-42-S indicates the SCGC mix having FA/S of 0.5, NaOH molarity of 8 M, Sp/P of 4 %, G/Glim 42 %, and silica sand as a fine aggregate.

2.3. Mixing, casting, and testing of specimen

The sodium hydroxide (NaOH) and sodium silicate (Na_2SiO_3) based alkaline solution was prepared 24 h before casting. The coarse aggregates were soaked in water for 24 h and their surface was dried before mixing to bring them to saturated surface dry condition. The fly ash and sand were initially dry mixed for 1 min followed by the wet mixing with the addition of an alkaline activator and mixing was continued for another 2 min. The extra water and superplasticizer were added together, and mixing was continued for further 2 min. Finally, coarse aggregates were added, and mixing was continued for 1 min. The flow deformability of each SCGC mix was determined using slump cone apparatus as per the guidelines of the European Federation of National Associations Representing for Concrete (EFNARC) [45]. To measure the flow speed and viscosity of each SCGC mix the time to reach 500 mm slump flow ($T_{500\ mm}$) was measured as per the recommendations of EFNARC [45]. The various stages for the mixing of SCGC are shown in Fig. 5. The filling ability and passing ability of SCGC were also determined by using standard V funnel apparatus, J ring apparatus and U box apparatus as per the recommendation of EFNARC [45] as shown in Fig. 6.

Cylindrical molds, 100 mm in diameter and 200 mm in height were filled with SCGC and placed at curing temperatures in a range of 60 °C to 80 °C. The heat-cured specimens were taken out from an oven after 24 h–48 h and demolded. SCGC specimens were then placed at ambient temperature (20 °C ± 2 °C) up to testing. The density of each SCGC mix were determined as per ASTM C138 [46].

Table 9
Volumetric proportion of self-compacting geopolymer concrete (SCGC) mixes for 1 m^3.

Sr. No.	Mix ID	Fly ash	Sand		Coarse Aggregate	NaOH		Na_2SiO_3	Extra water	Sp
		kg/m^3	Type	kg/m^3	kg/m^3	M	kg/m^3	kg/m^3	kg/m^3	kg/m^3
01	G-0.5-8-4-42-S	384	silica	767	678	8	66	164	38	15
02	G-0.5-10-4-42-S	384	silica	769	679	10	66	165	38	15
03	G-0.5-12-4-43-S	385	silica	771	681	12	66	165	39	15
04	G-0.5-14-4-43-S	386	silica	771	682	14	66	165	39	15
05	G-0.5-16-4-43-S	386	silica	772	683	16	66	166	39	15
06	G-1-12-3-43-S	528	silica	528	682	12	90	226	21	16
07	G-1-12-2-42-S	525	silica	525	678	12	90	225	32	11
08	G-1-16-3-43-S	530	silica	530	684	16	91	227	21	16
09	G-0.75-16-2-41-S	492	silica	656	656	16	84	211	15	10
10	G-0.75-14-2-41-S	491	silica	655	655	14	84	211	15	10
11	G-0.75-12-2-41-S	491	silica	654	654	12	84	210	15	10
12	G-0.75-16-0-41-S	497	silica	663	663	16	85	213	15	0
13	G-0.75-16-2-42-N	506	Natural	675	675	16	87	217	15	10
14	G-0.75-12-2-42-N	504	Natural	673	673	12	86	216	15	10
15	G-0.63-16-2-40-N	481	Natural	769	641	16	82	206	14	10
16	G-0.61-16-2-50-N	430	Natural	701	797	16	74	184	26	9
17	G-0.78-16-2-50-N	472	Natural	598	802	16	81	202	28	9

(a) fly ash and sand (b) dosage of alkaline solution (c) dosage of water and superplasticzer

(d) addition of coarse aggregate (e) fresh SCGC paste

Fig. 5. Various steps for preparation of SCGC mixes.

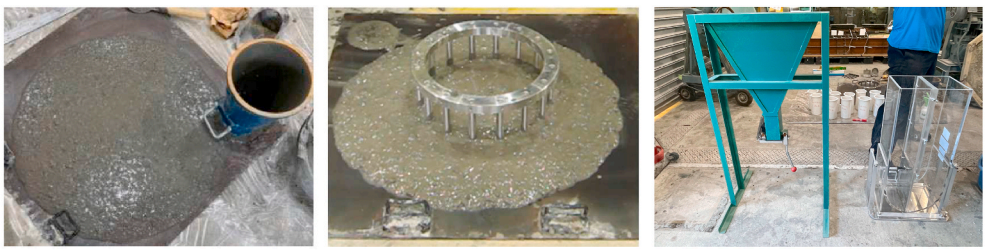

(a) Slump cone apparatus (b) J-ring apparatus (c) V funnel and U box apparatus

Fig. 6. Test equipment's for determination of flow properties of SCGC.

The compressive strength of each SCGC mix was determined by applying uniaxial compressive load at 7 d and 28 d of curing as per the recommendations of ASTM C39 [47].

The stress versus strain relationships was proposed based on the deformations results of attached strain gauges as shown in Fig. 7 (a). The strain gauges were attached in the longitudinal, and lateral direction to determine respective deflection, as shown in Fig. 7(a). The midpoint of the strain gauges, with a gauge length of 60 mm, was at the central height of the specimen (100 mm). The experimental arrangement used to measure the axial and lateral strains is illustrated in Fig. 6(b). Young's modulus and Poisson's ratio of SCGC were calculated as per the guidelines of ASTM C469 [48].

3. Results and discussions

3.1. Fresh mechanical properties

3.1.1. Comparison of flow parameters of SCC and SCGC

The parameters controlling the flow properties of SCC [1] were also calculated for SCGC. The coarse aggregate volume to solid volume (G/Glim) for SCGC was kept within a range of 40 %–50 %, whereas for SCC the G/Glim recommended value is 50 % [1]. The Vs/Vmortar for SCGC having silica sand and natural sand was within the range of 30 %–45 % and 33 %–39 % respectively as shown in Fig. 8. The comparatively lesser Vs/Vmortar ratio is required in SCGC to achieve comparable flow speed. The limited fine aggregate content in SCC is usually recommended to control shear deformability and pressure transformability. The degree of decrease in shear deformability in SCC mainly depends on the solid content in the mortar [1]. The flow deformability of SCGC having silica sand (mix G-0.5-16-4-43-S) and natural sand (mix G-0.61-16-2-50-N) is shown in Fig. 9. It was physically examined that the SCGC having silica sand looks more cohesive and viscous in comparison to SCGC having natural sand as shown in Fig. 9.

The volumetric ratio of paste (Vpaste) and volume of water to volume of powder ratio (Vw/Vp) for SCGC lie close to the recommended value of SCC as shown in Fig. 10. The SCGC having silica sand had Vpaste and Vw/Vp was within a range of 38 %–49 % and 0.87 to 1.11, respectively. Higher Vpaste with the lesser Vw/Vp was considered for SCGC having silica sand. The concept behind this was to control segregation [1]. Whereas SCGC having natural sand had Vpaste and Vw/Vp within the range of 40 %–45 % and 0.87 to 0.94, respectively as shown in Fig. 10. The comparatively lower significance of Vw/Vp in controlling the flow properties of SCGM compared to SCM is because of the high viscosity of alkaline activators [18].

3.1.2. Effect of NaOH molarity

The workability test results of each SCGC mix are shown in Table 10. The effect of NaOH molarity on the flow properties of SCGC was determined for mixes G-0.5-8-4-42-S, G-0.5-10-4-42-S, G-0.5-12-4-43-S, G-0.5-14-4-43-S, and G-0.5-16-4-43-S as shown in Fig. 11. The NaOH molarity had a clear impact on flow deformability and time to reach 500 mm slump flow ($T_{500\ mm}$). The slump flow of SCGC was about 750 mm, 750 mm, 700 mm, 700 mm, and 680 mm at NaOH molarity of 8 M, 10 M, 12 M, 14 M, and 16 M as shown in Fig. 11. The $T_{500\ mm}$ for SCGC was about 5 s, 5 s, 7 s, 8 s, and 10 s at NaOH molarity of 8 M, 10 M, 12 M, 14 M, and 16 M. The increase in NaOH molarity from 8 M to 16 M resulted in a decrease in flow deformability by 9.3 %, whereas $T_{500\ mm}$ was increased by 100 % with a rise in NaOH molarity from 8 M to 16 M. This proves that NaOH molarity had a more significant impact on flow speed in comparison to flow deformability. The test results exhibited that the increase in NaOH molarity resulted in an increase in the viscosity of geopolymer paste which had a negative impact on the flow speed. Similar findings were also observed in previous studies [18,19]. The flow deformability of SCGC for different NaOH molarities is shown in Fig. 12.

3.1.3. Effect of fly ash to sand ratio

The effect of fly ash to sand ratio (FA/S) on the flow properties of SCGC was determined as shown in Fig. 13. The increase in fly ash to sand ratio from 0.5 to 1.0, resulted in a continuous increase in flow deformability and a decrease in time to reach 500 mm slump flow ($T_{500\ mm}$). This might be because with an increase in FA/S chances of reduction in shear resistance increased due to a decrease in Vs/Vmortar [1]. The increase in fly ash content resulted in an increase in spherical shape particles due to which sliding between particles

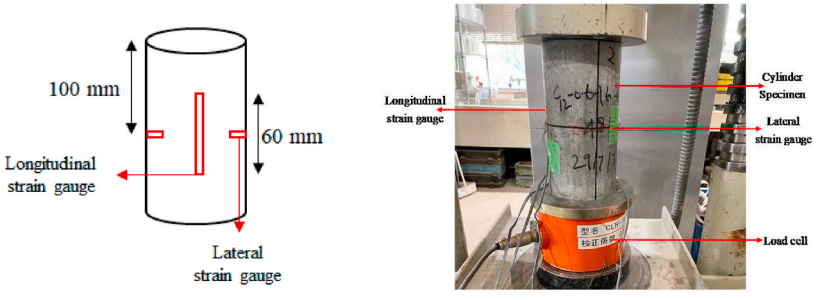

Fig. 7. Experimental test setup of compression for SCGC specimens with measurement of axial and lateral strain.

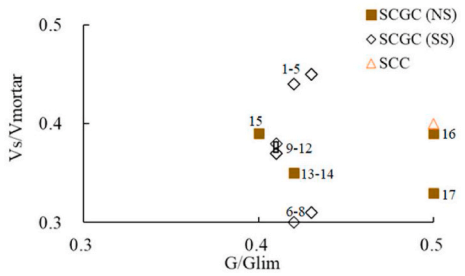

Fig. 8. Comparison of relationship between degree of compaction in coarse aggregate and volume of sand to mortar ratio in SCC and SCGC.

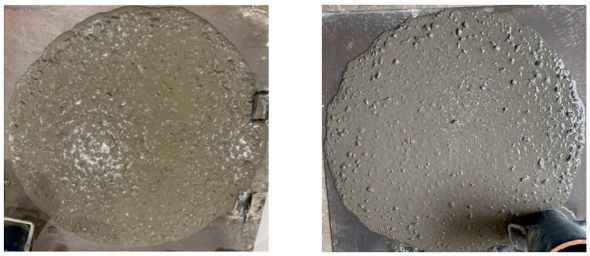

Fig. 9. Flow deformability of SCGC mixes.

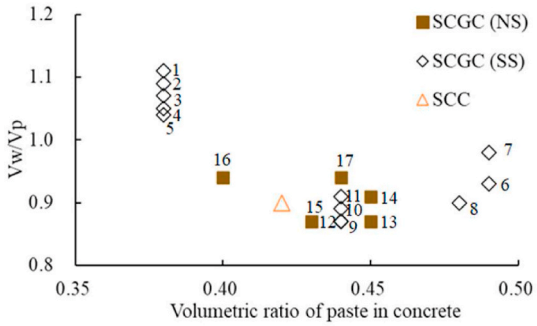

Fig. 10. Comparison of volumetric ratio of paste and volume of water to volume of powder ratio in SCC and SCGC.

increased [20,23,49]. The maximum slump flow of 785 mm and minimum $T_{500\ mm}$ of 4 s was achieved for SCGC mix G-1-12-2-42-S having fly ash to sand ratio 1.0, Vs/Vmortar of 30 %, W/GPS of 0.341, and Sp/P of 2 % as shown in Fig. 13. SCGC mix G-0.5-12-4-43-S contains a comparatively higher amount of superplasticizer compared to SCGC mix G-1-12-2-42-S, but the flow properties were comparatively low due to high Vs/Vmortar. This clarifies the significance of fly ash to sand ratio on the flow properties of SCGC. The increase in FA/S from 0.75 (mix G-0.75-12-2-41-S, mix G-0.75-14-2-41-S, mix G-0.75-16-2-41-S) to 1.0 (mix G-1-12-2-42-S, mix G-1-12-3-43-S, mix G-1-16-3-43-S) had a positive impact on the flow properties of SCGC as shown in Fig. 13. The increase in FA/S from 0.5 (mix G-0.5-12-4-43-S) to 0.75 (mix G-0.75-12-2-41-S) and a decrease in Sp/P from 4 % to 2 % resulted in an increase in flow deformability from 700 mm to 750 mm. This emphasizes the importance of FA/S on the flow deformability of SCGC compared to Vw/Vp and Sp/P.

The increase in FA/S from 0.61 (mix G-0.61-16-2-50-N) to 0.78 (mix G-0.78-16-2-50-N) resulted in an increase in slump flow from 690 mm to 705 mm and a decrease in $T_{500\ mm}$ 15 s–11 s as mentioned in Table 11. The flow passing time was also reduced from 25 s to 20 s with the increase in FA/S from 0.61 to 0.78. The SCGC mix had a higher content of Vs/Vmortar ratio showed a greater passing ability compared to the SCGC mix having lesser Vs/Vmortar as mentioned in Table 11.

3.1.4. Effect of superplasticizer and water

The impact of the superplasticizer in controlling the flow properties of SCGC was also important as shown in Fig. 13. The minimum slump flow of 665 mm with a maximum $T_{500\ mm}$ of 30 s was observed for SCGC mix G-0.75-16-0-41-S having no superplasticizer. The $T_{500\ mm}$ was decreased from 30 s (G-0.75-16-0-41-S) to 20 s (G-0.75-16-2-41-S) with the addition of the superplasticizer by 2 %. The

Table 10
Workability test results of SCGC.

Sr. No.	Mix ID	W/GPS*	G/Glim*	Vs/Vmortar*	Vpaste*	Slump Flow (Inverted)	T_{500mm} flow time (Inverted)
		Ratio	%	%	%	mm	s
01	G-0.5-8-4-42-S	0.393	42	44	38	750	5
02	G-0.5-10-4-42-S	0.383	42	44	38	750	5
03	G-0.5-12-4-43-S	0.374	43	45	38	700	7
04	G-0.5-14-4-43-S	0.365	43	45	38	700	8
05	G-0.5-16-4-43-S	0.358	43	45	38	680	10
06	G-1-12-3-43-S	0.325	43	31	49	760	5
07	G-1-12-2-42-S	0.341	42	30	49	785	4
08	G-1-16-3-43-S	0.310	43	31	48	745	7
09	G-0.75-16-2-41-S	0.302	41	37	44	700	20
10	G-0.75-14-2-41-S	0.309	41	37	44	710	17
11	G-0.75-12-2-41-S	0.317	41	37	44	750	11
12	G-0.75-16-0-41-S	0.302	41	38	44	665	30
13	G-0.75-16-2-42-N	0.302	42	35	45	735	14
14	G-0.75-12-2-42-N	0.317	42	35	45	755	8
15	G-0.63-16-2-40-N	0.302	40	39	43	655	19
16	G-0.61-16-2-50-N	0.326	50	39	40	690	15
17	G-0.78-16-2-50-N	0.326	50	33	44	705	11

*W/GPS=Water to geopolymer solid; W = Total water (kg); GPS= Fly ash + NaOH(s) + Na_2SiO_3(s).
*G/Glim = Coarse aggregate volume to solid volume *Vs/Vmortar = volume of sand to volume of mortar ratio, *Vpaste = Vfly ash + vAlkaline solution + Vextra water + Vsp.

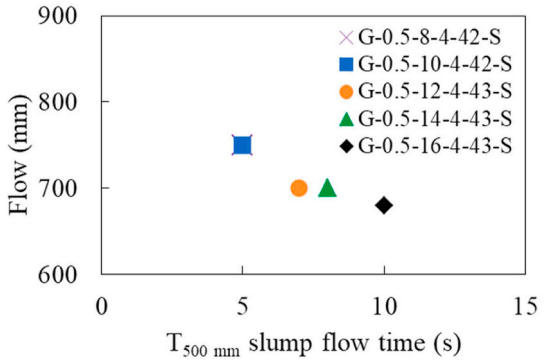

Fig. 11. Effect of sodium hydroxide concentration on flow properties of SCGC.

correlation between slump flow and $T_{500\ mm}$ proves that the flow speed of SCGC mainly depends on FA/S, Vw/Vp, and Sp/P. The impact of water to geopolymer solid ratio (W/GPS) on the flow properties of SCGC was also significant besides superplasticizer. The SCGC mix (G-1-12-2-42-S) had W/GPS of 0.341 and Sp/P of 2 % comparatively good flow properties compared to the SCGC mix (G-1-12-3-43-S) having W/GPS of 0.325 and Sp/P of 3 %. This also proves the importance of the Vw/Vp in controlling the viscosity of SCGC. A similar trend was observed in the previous study [18]. The Vw/Vp is also very important in SCC as self-compactibility mainly depends on this parameter [4].

3.1.5. Effect of natural sand and silica sand on flow properties

The effect of the type of sand on the flow properties of SCGC was also investigated as shown in Fig. 14. The replacement of natural sand improves the flow properties of SCGC as shown in Fig. 14. The flow deformability was increased from 750 mm (mix G-0.75-12-2-41-S) to 755 mm (mix G-0.75-12-2-42-N) and $T_{500\ mm}$ was decreased from 11 s to 8 s at NaOH molarity 12 M with the replacement of silica sand by natural sand keeping in view all other parameters as constant as mentioned in Table 10. Similarly, at NaOH molarity of 16 M, the $T_{500\ mm}$ of 20 s (mix G-0.75-16-2-41-S) was reduced to 14 s (mix G-0.75-16-2-42-N) with the replacement of silica sand with natural sand. This might be because the silica sand ultimately increased the silica content (SiO_2) which affects the flow properties by increasing the viscosity of the system [41]. The test results exhibited that the replacement of silica sand with natural sand had a clear influence on the flow speed of SCGC compared to flow deformability as shown in Fig. 14. The comparison of flow properties (flow deformability and flow speed) between SCGC and SCC is shown in Fig. 15. The test results exhibited that for the same flow deformability, the $T_{500\ mm}$ of SCC was comparatively much lower compared to SCGC. This is because of the high viscosity of geo-polymer paste due to which the effect of Vw/Vp and Sp/P was not much significant [18]. The test results exhibited that the flow deformability of SCGC lies within a similar range of SCC [5,50,51] however, $T_{500\ mm}$ of each SCGC mix was comparatively higher than SCC.

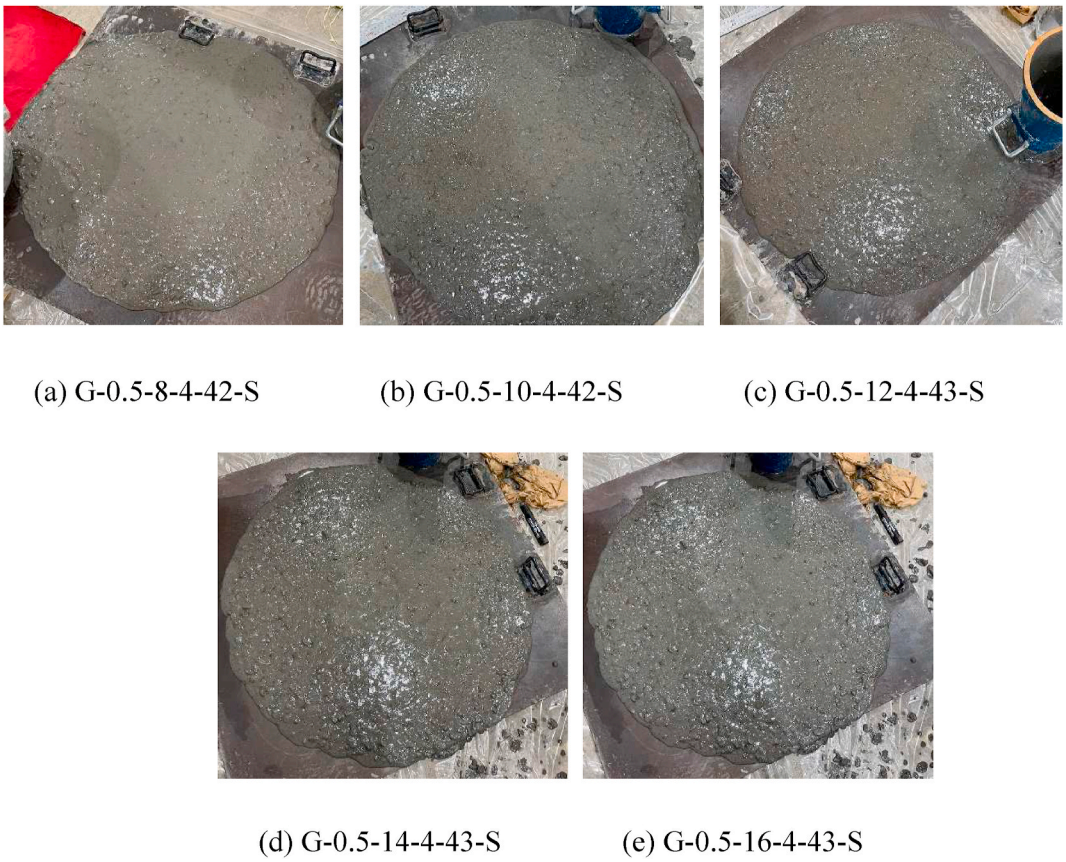

Fig. 12. Flow deformability of SCGC mixes based on the variation of NaOH molarity.

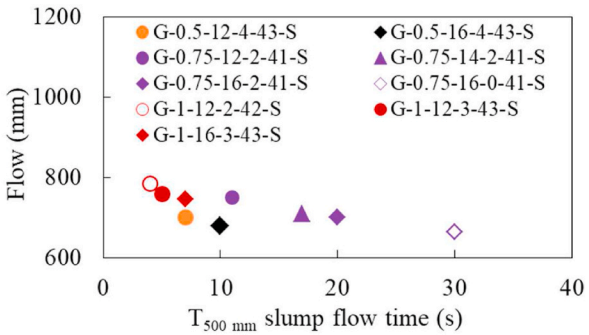

Fig. 13. Relationship between slump flow and time to reach 500 mm slump flow for SCGC.

Table 11
Comparison of various flow properties based on the variation of fly ash and sand content.

Mix ID	Slump flow (Inverted)	$T_{500\ mm}$ slump flow (Inverted)	V funnel flow	U-Box Height (Rank 2)	J-ring blocking step
	mm	s	s	mm	mm
G-0.61-16-2-50-N	690	15	25	365	5
G-0.78-16-2-50-N	705	11	20	340	5

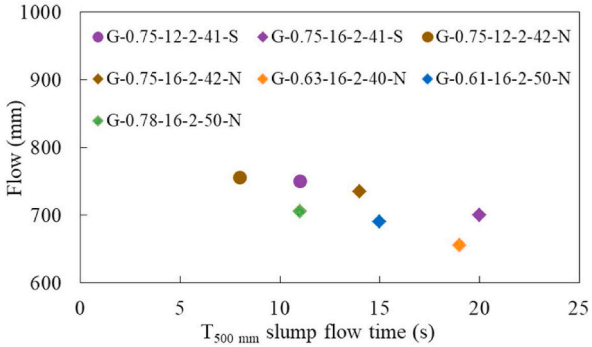

Fig. 14. Relationship between slump flow and time to reach 500 mm slump flow for SCGC based on the variation of type of sand and comparison with SCC.

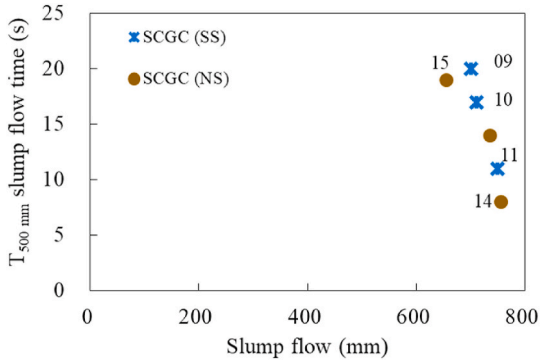

Fig. 15. Comparison between slump flow and time to reach 500 mm slump flow for SCGC based on the variation of type of sand and comparison with SCC.

3.2. Hardened state properties

3.2.1. Dry density

3.2.1.1. Effect of NaOH molarity and curing time. The impact of NaOH molarity on the dry density of SCGC was determined as mentioned in Table 12. No clear trend was observed in the density of SCGC based on the variation of NaOH molarity. The increase in NaOH molarity generally improves the microstructure of geopolymer [9]. The maximum dry density of 2266 kg/m^3 was found for SCGC mix G-0.5-14-4-43-S whereas a minimum dry density of 2196 kg/m^3 was achieved for SCGC mix G-0.5-8-4-42-S. This might be because of the change in the microstructure of the geopolymer due to a change in NaOH molarity [9].

The test results exhibited that with an increase in curing time from 24 h to 48 h the dry density was reduced as shown in Fig. 16. This might be because of continuous evaporation of water with an increase in curing duration [41,52]. The dry density of SCGC mixes lies within a range of 2211 kg/m^3 to 2266 kg/m^3 for SCGC specimens cured for 24 H at 80 °C, whereas dry density lies within the range of 2196 kg/m^3 to 2239 kg/m^3 for SCGC specimens cured for 48 H at 80 °C as shown in Fig. 16.

3.2.1.2. Effect of curing temperature. The effect of curing temperature on the dry density of SCGC was also determined as shown in Fig. 17. The rise in curing temperature from 60 °C to 70 °C resulted in a decrease in the dry density of SCGC. The increase in curing temperature from 60 °C to 70 °C resulted in a decrease in dry density from 2218 kg/m^3 to 2212 kg/m^3 and 2216 kg/m^3 to 2154 kg/m^3 for SCGC mix G-1-12-3-43-S and mix G-1-12-2-42-S, respectively. This might be because of acceleration in the geopolymerization phenomena and possibility of evaporation due to an increase in temperature [41,52].

3.2.1.3. Effect of curing age. The effect of age on the dry density of SCGC was determined by measuring the dry density at 7 d and 28 d as shown in Fig. 18. The increase in curing age from 7 d to 28 d resulted in a decrease in dry density as shown in Fig. 18. The dry density was decreased from 2270 kg/m^3 to 2253 kg/m^3 and from 2262 kg/m^3 to 2220 kg/m^3 for SCGC mix G-0.61-16-2-50-N and mix G-0.78-16-2-50-N, respectively with an increase in age from 7 days to 28 days. Previous studies also reported a similar trend [36,53]. This might be because of the continuous evaporation over time [54] Overall test results depict that the dry density of SCGC lies within the range (2155 kg/m^3 to 2560 kg/m^3) of ACI building code [55].

Table 12
Experimental results of mechanical properties of SCGC.

Sr. No.	Mix ID	Curing Temperature	7 Days dry density	28 Days dry density	7 Days compressive strength	28 Days compressive strength	Segregation	Youngs Modulus GPa		Poisson's ratio	
		°C	kg/m^3		MPa		mm	7	28	7	28
01	G-0.5-8-4-42-S	24 H 80 48 H 80	2260 2196	–	5 8	–	30	–			
02	G-0.5-10-4-42-S	24 H 80 48 H 80	2236 2208	–	6 10	–	30	–			
03	G-0.5-12-4-43-S	24 H 80 48 H 80	2232 2239	–	9 10	–	30	–			
04	G-0.5-14-4-43-S	24 H 80 48 H 80	2266 2223	–	11 14	–	30	–			
05	G-0.5-16-4-43-S	24 H 80 48 H 80	2211 2220	–	14 17	–	30	–			
06	G-1-12-3-43-S	48 H 60 48 H 70	2218 2212	–	19 23	–	60 90	–			
07	G-1-12-2-42-S	48 H 60 48 H 70	2216 2154	–	17 21	–	40 90	–			
08	G-1-16-3-43-S	48 H 60 48 H 70	2217 2222	–	26 25	–	40 70	–			
09	G-0.75-16-2-41-S	48 H 80	2264	–	37	–	60	–			
10	G-0.75-14-2-41-S	48 H 80	2246	–	37	–	60	–			
11	G-0.75-12-2-41-S	48 H 80	2240	–	29	–	60	–			
12	G-0.75-16-0-41-S	48 H 80	2220	–	36	–	15	–			
13	G-0.75-16-2-42-N	48 H 80	2190	–	27	–	0	–			
14	G-0.75-12-2-42-N	48 H 80	2185	–	21	–	0	–			
15	G-0.63-16-2-40-N	48 H 80	2177	–	27	–	0	–			
16	G-0.61-16-2-50-N	48 H 80	2270	2253	25	27	0	14.7	15.2	0.19	0.18
17	G-0.78-16-2-50-N	48 H 80	2262	2220	25	26	0	14.5	14.9	0.18	0.17

3.2.2. *Compressive strength*

3.2.2.1. Effect of NaOH molarity. The effect of NaOH molarity on the compressive strength of SCGC was determined by varying NaOH molarity from 8 M to 16 M as shown in Fig. 19. The increase in NaOH molarity from 8 M (mix-G-0.5-8-4-42-S) to 16 M (mix-G-0.5-16-4-43-S) for SCGC specimens cured for 24 h at 80 °C resulted in an increase in 7 days compressive strength from 5 MPa to 14 MPa as shown in Fig. 19. Similarly, SCGC specimens cured for 48 h at 80 °C with an increase in NaOH molarity from 8 M (mix-G-0.5-8-4-42-S) to 16 M (mix-G-0.5-16-4-43-S) resulted in an increase in 7 d compressive strength from 8 MPa to 17 MPa. The maximum compressive strength of 17 MPa was achieved for SCGC mix-G-0.5-16-4-43-S having a NaOH molarity of 16 M. The average increase in compressive strength was about 25 %, 40 %, and 21 %, with an increase in NaOH molarity from 8 M to 10 M, 12 M–14 M, and 14 M–16 M, respectively. This is because with an increase in NaOH molarity geopolymerization phenomena accelerated owing to the dissolution of silica and alumina particles from binder [9,41]. The increase in dissolution resulted in an increase in the formation of sodium aluminum silicate hydrate gel (*N*-A-*S*-H) which ultimately resulted in a dense microstructure [22].

3.2.2.2. Effect of fly ash to sand ratio. The impact of fly ash to sand ratio (FA/S) on the compressive strength of SCGC was determined

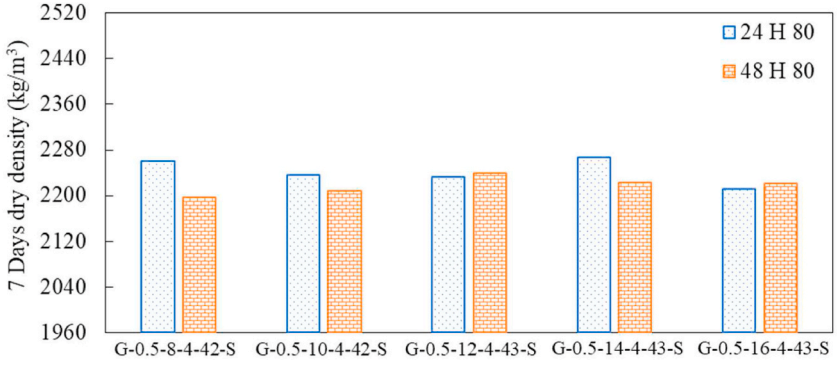

Fig. 16. Effect of NaOH molarity and curing duration on 7 days dry density of SCGC.

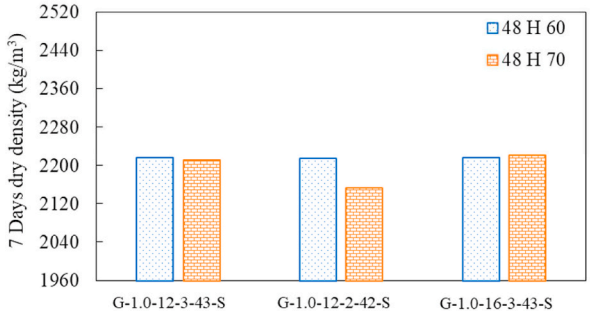

Fig. 17. Effect of curing temperature on 7 days dry density of SCGC.

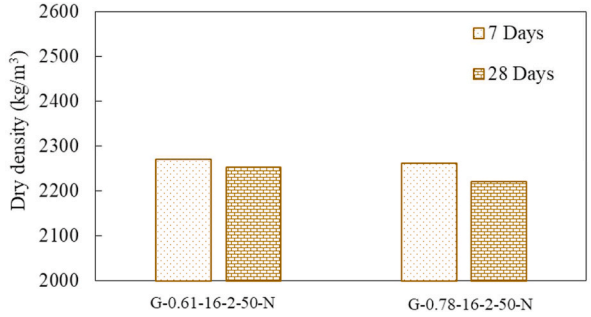

Fig. 18. Comparison between 7 days and 28 days dry density of SCGC.

as shown in Fig. 20. The increase in fly ash to sand ratio from 0.5 (G-0.5-12-4-43-S) to 0.75 (G-0.75-12-2-41-S) and a decrease in Sp/P from 4 % to 2 % resulted in an increase in compressive strength from 10 MPa to 29 MPa at NaOH molarity 12 M. Similarly, the increase in fly ash to sand ratio from 0.5 (G-0.5-16-4-43-S) to 0.75 (G-0.75-16-2-41-S) and decrease in Sp/P from 4 % to 2 % resulted in an increase in compressive strength from 17 MPa to 37 MPa at NaOH molarity of 16 M. This is because with an increase in fly ash content resulted in an increase in binder ratio which had a strong influence on the strength development and the microstructure of GPC [15]. Moreover, with an increase in fly ash content, chances of the formation of sodium aluminum silicate hydrate gel (*N*-A-*S*-H) would increase resulting in a dense microstructure [20]. The more the formation of *N*-A-*S*-H results higher will be compressive strength of GPC [22]. A similar trend was also observed for normal GPC [20]. The optimum compressive strength of 37 MPa was achieved for SCGC mix G-0.75-16-2-41-S having G/Glim 41 %, Vs/Vmortar 37 %, and volume of paste 44 %.

3.2.2.3. Effect of type of fine aggregate. The effect of the type of fine aggregate on the compressive strength of SCGC was also investigated as shown in Fig. 21. Interestingly, it was found that the same volumetric proportion of constituents with a change in the type of sand also had an impact on the compressive strength of SCGC. Silica sand had a positive impact on the compressive strength of SCGC compared to natural sand. The compressive strength of SCGC having silica sand (mix G-0.75-12-2-41-S) was about 29 MPa which is reduced to 21 MPa with the replacement of silica sand with natural sand (mix G-0.75-12-2-42-N) as shown in Fig. 21. Similarly, the

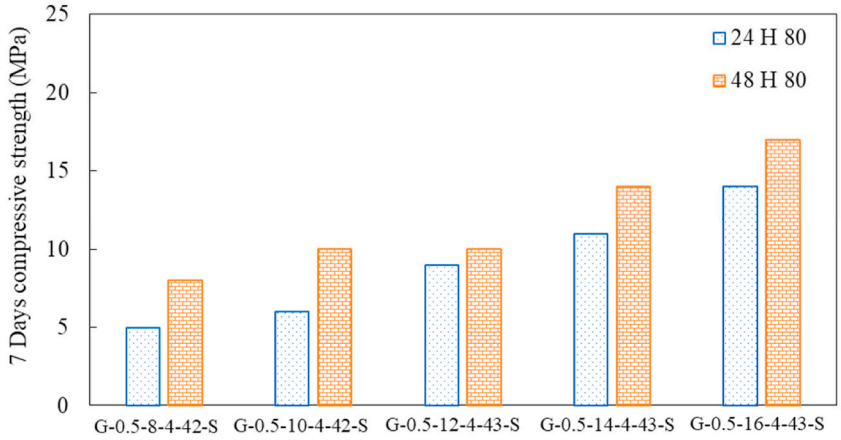

Fig. 19. Effect of NaOH molarity on 7 days compressive strength of SCGC.

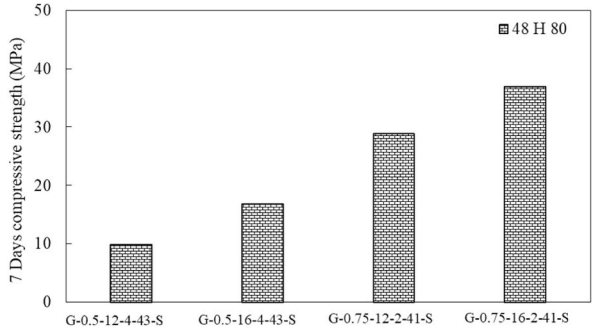

Fig. 20. Effect of fly ash to sand ratio on 7 days compressive strength of SCGC.

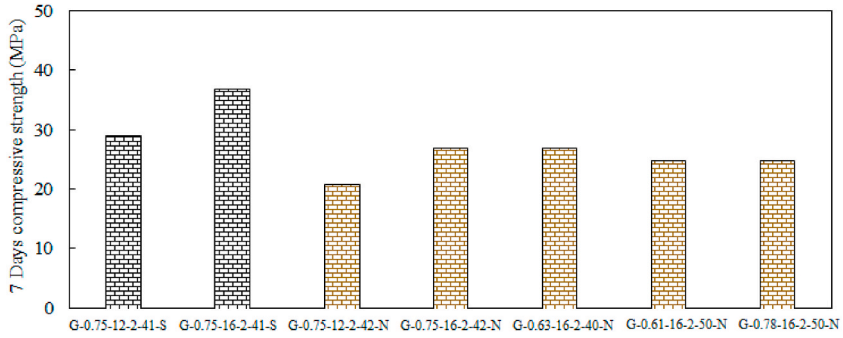

Fig. 21. Effect of type of sand on 7 days compressive strength of SCGC.

compressive strength of 37 MPa (mix G-0.75-16-2-41-S) was reduced to 27 MPa (G-0.75-16-2-42-N) with the replacement of silica sand with natural sand as shown in Fig. 21. This might be because of the higher content of silica which strongly effect the geopolymerization reaction [41]. The biggest advantage of replacing silica sand with natural sand is that it can entirely reduce the chances of segregation as mentioned in Table 12. The higher particle density of SCGM indicating the possible reason for segregation is because of the difference in the particle density of natural and silica sand. Natural sand has comparatively higher particle density that provided support against the sinking of coarse aggregate [41]. The fineness modulus of silica sand and natural sand was about 2.5 and 2.8, respectively indicating fine and medium sand. Moreover, the solid contents in both types of sand were almost the same indicating the possible reason for segregation is a difference in densities. The vertical cross-section of a tested specimen of SCGC having silica sand and natural sand is shown in Fig. 22.

The pictorial representation of the mechanism of segregation for SCGC having silica sand is shown in Fig. 23. The SCGC having silica sand had comparatively good viscosity in the fresh stage, however, during geopolymerization reaction lighter particles of fly ash

(a) Silica sand (b) Natural sand

Fig. 22. Vertical cross section of tested specimens of SCGC.

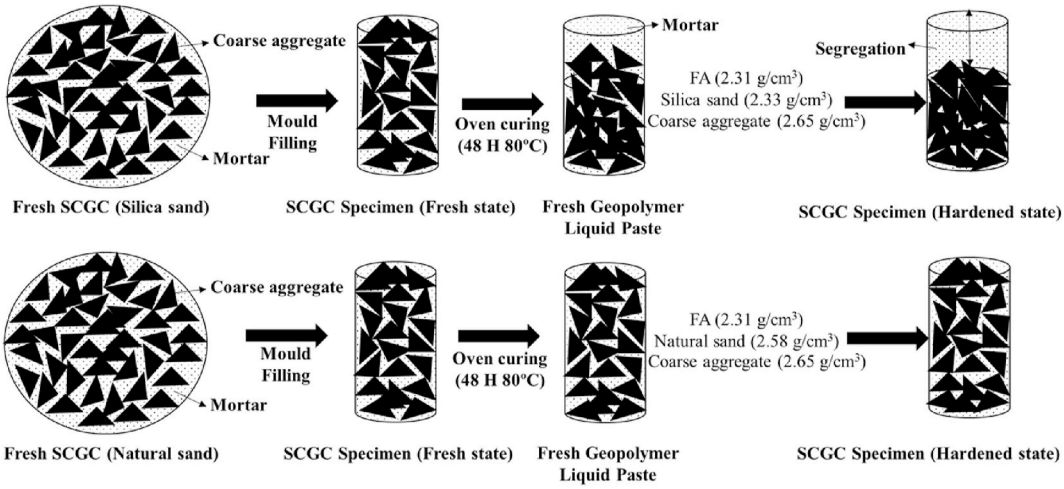

Fig. 23. Clarification of mechanism of segregation in SCGC based on the variation of type of sand.

and silica sand caused segregation as shown in Fig. 23. No segregation was observed in the fresh and hardened stage in SCGC based on the replacement of silica sand with natural sand as explained in Fig. 23.

3.2.2.4. Effect of curing temperature and curing age. The effect of curing temperature on the compressive strength of SCGC was also determined as shown in Fig. 24. The rise in curing temperature from 60 °C to 70 °C resulted in an increase in compressive strength. The

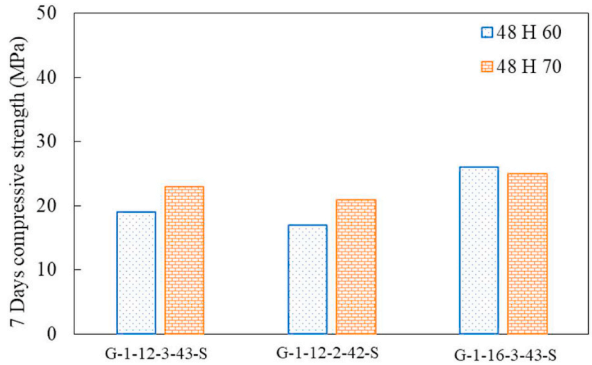

Fig. 24. Effect of curing temperature on 7 days compressive strength of SCGC.

increase in compressive strength with an increase in curing temperature was clear especially at a lower NaOH molarity of 12 M as shown in Fig. 24. This is because of the acceleration of the geopolymer reaction as a result of the activation of alumino silicate particles [56]. The increase in curing temperature converts the larger diameter pores into a uniform size which ultimately produces a dense microstructure [57]. The rate of exothermic reaction of GPC mainly depends on the curing temperature, therefore, curing temperature is the most significant factor that effect the compressive strength of GPC [26]. The curing temperature acts as a reaction accelerator in fly ash-based geopolymer and is one of the most important parameters controlling the compressive strength of geopolymers [58].

The impact of curing age on the compressive strength of SCGC was also determined by measuring the compressive strength at 7 d and 28 d as shown in Fig. 25. It was found that there is no significant difference in the 7 d and 28 d compressive strength of SCGC. The compressive strength of SCGC mix G-0.61-16-2-50-N was minorly increased from 25 MPa to 27 MPa with an increase in curing age from 7 days to 28 days. Similarly, for SCGC mix G-0.78-16-2-50-N the compressive strength was only increased by 1 MPa with an increase in curing age from 7 days to 28 days. This is because of heat curing due to which geopolymer concrete achieve maximum strength at initial stages. Similar findings were reported in a previous study [26]. The impact of curing age on the strength development of normal SCC based on some previous studies [4,59] is also shown in Fig. 25. The compressive strength of SCC was found to be higher than SCGC as shown in Fig. 25. The increase in compressive strength with an increase in age from 7 days to 28 days was significant for SCC compared to SCGC as presented in Fig. 25. This is because of the heat curing for 48 h at 60 °C–70 °C. A similar trend was also reported in a previous study [26].

3.2.2.5. Stress–strain curve. The relationship between stress versus axial strain and the stress versus lateral strain for SCGC was proposed with determination of axial and lateral deformation at age of 7 d and 28 d as shown in Figs. 26 and 27. All specimens of each SCGC mix represent a good relationship between stress and strain, as shown in Figs. 26 and 27. The continuous increase in stress was observed with an increase in axial and lateral strains, similar to OPC concrete. The ultimate axial strain corresponding to ultimate stress lies within the range of 1957 microstrain to 2612 microstrain and the ultimate lateral strain corresponding to ultimate stress lies within the range of 1298 microstrain to 1626 microstrain for SCGM mix G-0.61-16-2-50-N at the age of 7 d as shown in Fig. 26 (a). However, at the age of 28 days, the ultimate axial strain corresponding to ultimate stress lies within the range of 2328 microstrain to 3013 microstrain, and the ultimate lateral strain corresponding to ultimate stress lies within the range of 319 microstrain to 1905 microstrain as shown in Fig. 26 (b). The SCGM mix G-0.78-16-2-50-N ultimate axial strain lies within the range of 2161 microstrain to 2738 microstrain and the ultimate lateral strain lies within the range of 1558 microstrain to 2011 microstrain as shown in Fig. 27 (a). At the age of 28 days, the ultimate axial strain lies within the range of 2924 microstrain to 3270 microstrain and the ultimate lateral strain was within the range of 2009 microstrain to 2969 microstrain as shown in Fig. 27 (b). The increase in FA/S resulted in an increase in ultimate axial and lateral strain which proves the increase in chances of flexibility as shown in Fig. 28. The ductility of SCGM was also increased with an increase in fly ash content [36]. The SCGC specimen having lesser fly ash to sand ratio depicts more stiffness as shown in Fig. 28. Similar trend was also observed for SCGM in a previous study [36]. The stress–strain curves of SCGC show a sudden drop in stress after the ultimate point which means that failure was brittle having no strain hardening as shown in Figs. 26 and 27. This might be because of high-temperature curing and the ceramic nature of geopolymer [32]. Similar results were stated in a previous study [60]. The ultimate axial strain of SCGC lies well close to the general range for conventional OPC concrete (2000 με −3000με).

3.2.2.6. Young's modulus and Poisson's ratio. Young's modulus of SCGC was determined using the axial stress–strain curves recommended by ASTM C469 [48], as listed in Table 12. The comparison of Young's modulus of SCGM, SCGC, GPC, and OPC concrete (ACI 318) is shown in Fig. 29. Young's modulus of SCGC mixes lies within the range of 14.03 GPa–15.99 GPa as shown in Fig. 29. Young's modulus of SCGC was found lower than OPC of similar compressive strength. Previous studies found that Young's modulus of GPC [22,28,33,61] was lower than OPC concrete [55]. This is because of the lower Young's modulus of geopolymer paste [32]. Young's modulus of SCC was also lesser than OPC concrete due to the limited amount of coarse aggregates [5]. Earlier studies reported Young's modulus for GPC in a similar range of SCGC as shown in Fig. 29. However, some studies depict higher Young's modulus compared this study [22,33]. This might be because of the presence of a higher amount of water and superplasticizer as their presence affects the percentage of voids [22]. The OPC concrete Young's modulus can be determined using Eq. (1) as per ACI 318 [55]. Where α is 4.7 and fc' is the compressive strength in MPa.

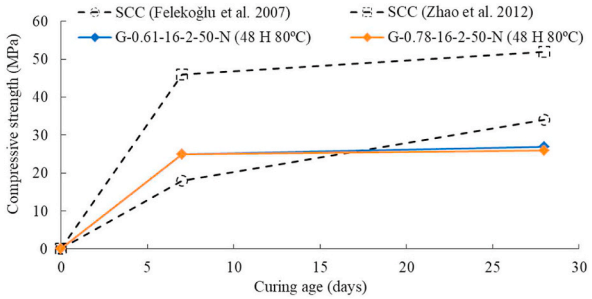

Fig. 25. Effect of curing age on the compressive strength of SCGC.

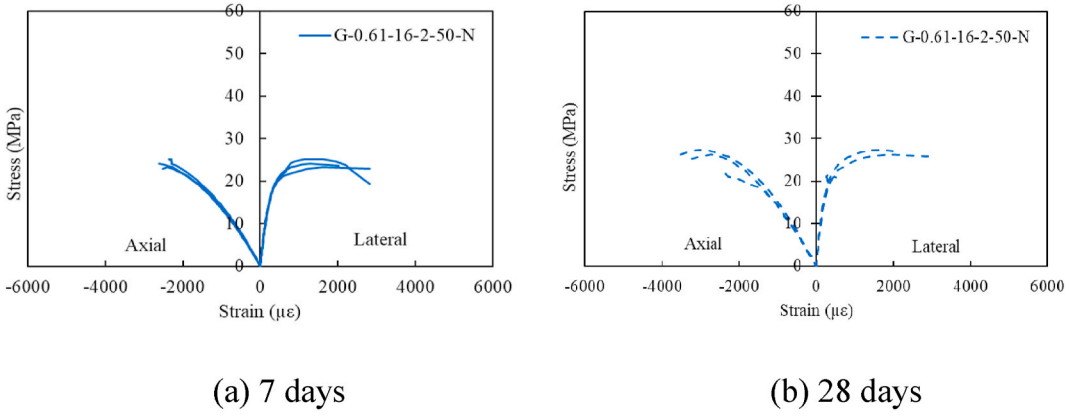

Fig. 26. Relationship between stress versus axial strain and stress versus lateral strain for SCGC mixes G-0.61-16-2-50-N.

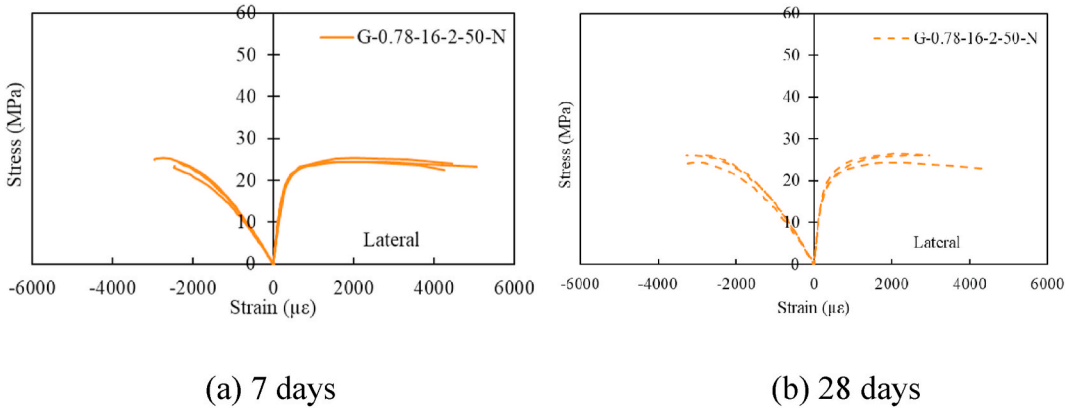

Fig. 27. Relationship between stress versus axial strain and stress versus lateral strain for SCGC mix G-0.78-16-2-50-N.

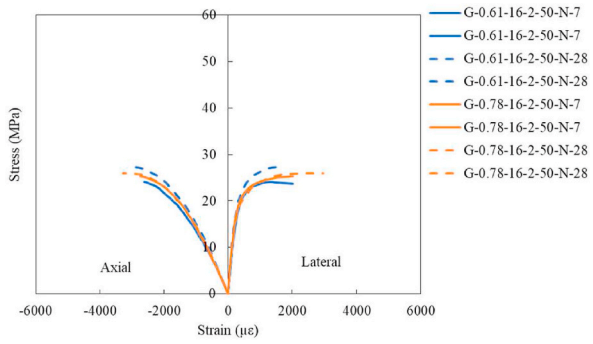

Fig. 28. Comparison of stress versus axial strain and stress versus lateral strain curves of SCGC mixes.

$$E(GPa) = \alpha \times \left(\sqrt{fc'}\right) \tag{1}$$

The predicted Young's modulus of SCGC can be determined based on its compressive strength using the ACI 318–14 [55] Eq. (1). Where α is 3.0 and fc' is the compressive strength of SCGC in MPa. The maximum difference between the experimental and analytical expression is 6.75 %. The proposed equation results of Young's modulus of SCGC are very close to the previous studies conducted on GPC [28]. A mathematical equation to compute Young's modulus of previous geopolymer studies is shown in Fig, where α is about 4.0, 3.51, 2.90, 1.25, 1.75, and 0.85 based on previous studies [22,28,33,36], and [61].

The Poisson's ratio of SCGC mixes was also determined by taking the ratio of lateral to axial deformations at 40 % of ultimate stress

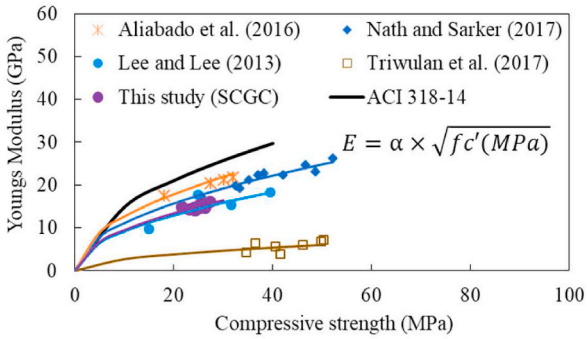

Fig. 29. Relationship between compressive strength and Young's modulus of SCGC.

[48] as mentioned in Table 12. The Poisson's ratio of SCGC lies within the range of 0.15–0.20 as shown in Fig. 30. There is no clear trend in Poisson's ratio based on the variation of influencing parameters. The Poisson's ratio of SCGC lies within a range of OPC concrete [62]. The Poisson's ratio of OPC concrete ranges from 0.11 to 0.21 [62]. Poisson's ratio of SCGC is within the recommended range of normal GPC based on previous studies [15,60].

4. Mix design processing

The mix design flow chart for self-compacting geopolymer concrete (SCGC) is proposed based on the experimental test results as shown in Fig. 31. The mix design for SCGC is proposed for silica sand and natural sand separately. The mix design for SCGC is proposed by fixing various boundary conditions.

The boundary conditions to develop a mix design for SCGC include aggregate specific conditions, mixing speed, mixing time, mixing temperature, curing temperature, and Na_2O/SiO_2 molar ratio as shown in Fig. 31. Previous study also highlighted the significance of many parameters to attain desired workability and strength for GPC. It was found that mixing time and speed had an effect on the workability of GPC [63]. The recommended way is to utilize aggregate content in saturated surface dry conditions. The high-viscosity geopolymer paste demanded a specific mixing speed and mixing time. The mixing temperature also had an impact on the flow and setting time properties of SCGC. The previous study investigated that the setting type of SCGC depends on the type of binder [37].

The mixing at temperatures below 20 °C resulted in the quick hardening of SCGC paste, especially at high molarity of NaOH. The flash setting was observed during mixing for SCGC having sodium oxide to silica molar ratio (Na_2O/SiO_2) beyond 0.169. The alkaline activator to fly ash ratio (AA/FA) was kept constant at 0.6, Na_2SiO_3/NaOH ratio at 2.5, and volume of air (V_{air}) at 3 %. The superplasticizer to powder ratio (Sp/P), extra water to powder ratio (W_{ex}/P), and volume of water to volume of powder ratio (Vw/Vp) was decided in step 2. Thirdly alkaline activator concentrations (NaOH and Na_2SiO_3) were chosen considering their impact on the flow properties and compressive strength. NaOH molarity was kept constant at 16 M to achieve a compressive strength of more than 25 MPa. The water to geopolymer solid ratio (W/GPS) was also decided based on its impact on fresh and hardened mechanical properties. Fourthly, limiting values of influencing parameters for normal SCC [1] were decided including coarse aggregate volume to its solid volume (G/Glim), the volume of sand to volume of mortar (Vs/Vmortar), and the volume of paste (Vpaste).

The flow chart indicating various influencing parameter is shown in Fig. 31. The mix design for fly ash-based SCGC is proposed considering flow deformability of greater than 680 mm with 7 days compressive strength of more than 25 MPa.

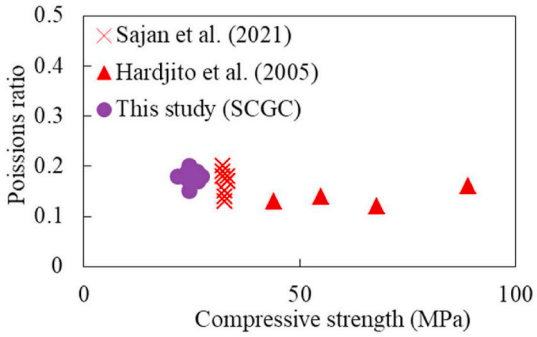

Fig. 30. Relationship between compressive strength and Poisson's ratio of SCGC.

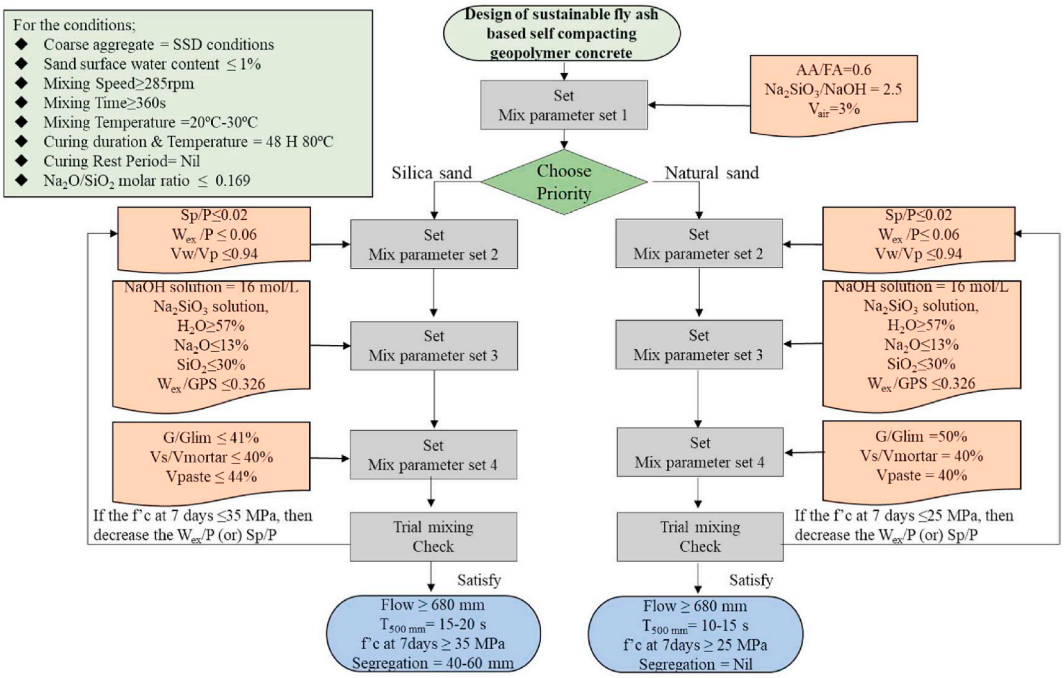

Fig. 31. Mix design flow chart for self-compacting geopolymer concrete (SCGC).

5. Conclusions

In this experimental study, seventeen (17) SCGC mixes were cast to investigate the impact of various influencing parameters on the fresh and hardened state mechanical properties of SCGC. Following are the conclusions based on this research study.

1. The increase in NaOH molarity from 8 M to 16 M had an impact on the flow properties of SCGC. The slump flow of 750 mm was decreased to 680 mm, whereas the time to reach 500 mm slump flow ($T_{500\ mm}$) was increased from 5 s to 10 s with a rise in NaOH molarity from 8 M to 16 M. The increase in fly ash to sand ratio (FA/S) had a positive impact on the flow properties of SCGC.
2. The replacement of silica sand with natural sand had an impact on the flow speed of SCGC in comparison to flow deformability due to difference in rate of geopolymerization due to variation of silica content. The $T_{500\ mm}$ was reduced from 11 s to 8 s and 20 s–14 s at NaOH molarity of 12 M, and 16 M, respectively, with the replacement of silica sand with natural sand.
3. The increase in NaOH molarity from 8 M to 16 M resulted in a continuous increase in the compressive strength of SCGC. The maximum compressive strength of 37 MPa was achieved for the SCGC mix cured for 48 H at 80 °C, having a NaOH concentration of 16 M, and FA/S of 0.75.
4. The replacement of silica sand with natural sand controls the segregation; however, natural sand had negatively affected the compressive strength of SCGC in comparison to silica sand. The compressive strength of 37 MPa was reduced to 27 MPa by the replacement of silica sand with natural sand.
5. The ultimate axial strain corresponding to the ultimate stress of SCGC lies within the recommended range of OPC concrete. Young's modulus of SCGC was found lower than OPC concrete. However, Poisson's ratio lies well within the range of OPC concrete.
6. The mix design flow chart for SCGC is proposed based on the experimental test results indicating different influencing parameters.

Data availability statement

Data will be made available on request.

Additional information

No additional information is available for this paper.

CRediT authorship contribution statement

M. Talha Ghafoor: Writing – original draft, Methodology, Investigation, Formal analysis, Data curation, Conceptualization. **Chikako Fujiyama:** Writing – review & editing, Validation, Supervision, Funding acquisition, Conceptualization.

Declaration of competing interest

The authors declare that they have no known conflicting financial interests or personal connections that could have seemed to affect the work reported in this paper.

Acknowledgement

This work was supported by JSPS KAKENHI (grant number 22H00230).

Notation

AA/FA Alkaline activator to fly ash ratio by weight
ACI American Concrete Institute
FA/S Fly ash to sand ratio by weight
G/Glim Coarse aggregate volume to solid volume
GPS Geopolymer solid (fly ash + alkaline activator solid)
$Na_2SiO_3/NaOH$ Sodium silicate to sodium hydroxide
Na_2O/SiO_2 Sodium oxide to silica molar ratio
Sp/P Superplasticizer to powder ratio by weight
SCGC (SS) Self-compacting geopolymer concrete having silica sand
SCGC (NS) Self compacting geopolymer concrete having natural sand
Vpaste Volume of paste (Vfly ash + vAlkaline solution + Vextra water + Vsp)
Vs/Vmortar Volume of sand to volume of mortar ratio
Vw/Vp Volume of water to volume of powder ratio
W/GPS Water to geopolymer solid ratio by weight
Wex/P Extra water to powder ratio by weight

References

[1] H. Okamura, M. Ouchi, Sel-compacting concrete, Vol.1, No.1, April 2003,", J. Adv. Concr. Technol. 1 (1) (2003) 5–15.
[2] A. Benli, Mechanical and durability properties of self-compacting mortars containing binary and ternary mixes of fly ash and silica fume, Struct. Concr. 20 (3) (2019) 1096–1108, https://doi.org/10.1002/suco.201800302.
[3] S. Hammat, B. Menadi, S. Kenai, C. Thomas, M.S. Kirgiz, A.G. de Sousa Galdino, The effect of content and fineness of natural pozzolana on the rheological, mechanical, and durability properties of self-compacting mortar, J. Build. Eng. 44 (2021), 103276, https://doi.org/10.1016/j.jobe.2021.103276.
[4] B. Felekoğlu, S. Türkel, B. Baradan, Effect of water/cement ratio on the fresh and hardened properties of self-compacting concrete, Build. Environ. 42 (4) (2007) 1795–1802, https://doi.org/10.1016/j.buildenv.2006.01.012.
[5] N. Abdizadeh, a Zekavati, H. Afshin, M. Student, Mix design of structural self-compacting concrete using void-bulk density method, Third Int. Conf. Concr. Dev. (2009) 999–1009 [Online]. Available: http://www.irbnet.de/daten/iconda/CIB13831.pdf.
[6] A. Attachaiyawuth, S. Rath, K. Tanaka, M. Ouchi, Improvement of self-compactability of air-enhanced self-compacting concrete with fine entrained air, J. Adv. Concr. Technol. 14 (3) (2016) 55–59, https://doi.org/10.3151/jact.14.55.
[7] S. Demie, M.F. Nuruddin, N. Shafiq, Effects of micro-structure characteristics of interfacial transition zone on the compressive strength of self-compacting geopolymer concrete, Construct. Build. Mater. 41 (2013) (2013) 91–98, https://doi.org/10.1016/j.conbuildmat.2012.11.067.
[8] O. Boukendakdji, E.H. Kadri, S. Kenai, Effects of granulated blast furnace slag and superplasticizer type on the fresh properties and compressive strength of self-compacting concrete, Cem. Concr. Compos. 34 (4) (2012) 583–590, https://doi.org/10.1016/j.cemconcomp.2011.08.013.
[9] K. Chen, W.T. Lin, W. Liu, Effect of NaOH concentration on properties and microstructure of a novel reactive ultra-fine fly ash geopolymer, Adv. Powder Technol. 32 (8) (2021) 2929–2939, https://doi.org/10.1016/j.apt.2021.06.008.
[10] E. Benhelal, E. Shamsaei, M.I. Rashid, Challenges against CO2 abatement strategies in cement industry: a review, J. Environ. Sci. (China) 104 (2021) 84–101, https://doi.org/10.1016/j.jes.2020.11.020.
[11] J. Xie, J. Wang, B. Zhang, C. Fang, L. Li, Physicochemical properties of alkali activated GGBS and fly ash geopolymeric recycled concrete, Construct. Build. Mater. 204 (2019) 384–398, https://doi.org/10.1016/j.conbuildmat.2019.01.191.
[12] M.C. Collivignarelli, A. Abbà, M. Carnevale Miino, G. Cillari, P. Ricciardi, A review on alternative binders, admixtures and water for the production of sustainable concrete, J. Clean. Prod. 295 (2021), https://doi.org/10.1016/j.jclepro.2021.126408.
[13] J. Davidovits, Properties of geopolymer cements, First Int. Conf. Alkaline Cem. Concr. (1994) 131–149.
[14] P. Zhang, Z. Gao, J. Wang, J. Guo, S. Hu, Y. Ling, Properties of fresh and hardened fly ash/slag based geopolymer concrete: a review, J. Clean. Prod. 270 (2020), 122389, https://doi.org/10.1016/j.jclepro.2020.122389.
[15] D. Hardjito, B.V. Rangan, Development and Properties of Low-Calcium Fly Ash-Based Geopolymer Concrete, vol. 94, Res. Rep. GC, 2005 [Online]. Available: http://www.geopolymer.org/fichiers_pdf/curtin-flyash-GP-concrete-report.pdf.
[16] M. Fareed Ahmed, M. Fadhil Nuruddin, N. Shafiq, Compressive strength and workability characteristics of low-calcium fly ash-based self-compacting geopolymer concrete, World Acad. Sci. Eng. Technol. 74 (February) (2011) 8–14, https://doi.org/10.5281/zenodo.1330481.
[17] G. Fang, W.K. Ho, W. Tu, M. Zhang, Workability and mechanical properties of alkali-activated fly ash-slag concrete cured at ambient temperature, Construct. Build. Mater. 172 (2018) 476–487, https://doi.org/10.1016/j.conbuildmat.2018.04.008.
[18] M.T. Ghafoor, C. Fujiyama, K. Maekawa, Mix design processing for self compacting geopolymer mortar, J. Adv. Concr. Technol. 19 (11) (2021) 1133–1147, https://doi.org/10.3151/jact.19.1133.
[19] M.T. Ghafoor, Q.S. Khan, A.U. Qazi, M.N. Sheikh, M.N.S. Hadi, Influence of alkaline activators on the mechanical properties of fly ash based geopolymer concrete cured at ambient temperature, Construct. Build. Mater. 273 (2021), 121752, https://doi.org/10.1016/j.conbuildmat.2020.121752.
[20] D. Singhal Parveen, M.T. Junaid, B.B. Jindal, A. Mehta, Mechanical and microstructural properties of fly ash based geopolymer concrete incorporating alccofine at ambient curing, Construct. Build. Mater. 180 (2018) (2018) 298–307, https://doi.org/10.1016/j.conbuildmat.2018.05.286.

[21] M. Thakur, S. Bawa, Materials today : proceedings self-compacting geopolymer concrete : a review, Mater. Today Proc. 59 (2022) 1683–1693, https://doi.org/10.1016/j.matpr.2022.03.400.
[22] A.A. Aliabdo, A.E.M. Abd Elmoaty, H.A. Salem, Effect of cement addition, solution resting time and curing characteristics on fly ash based geopolymer concrete performance, Construct. Build. Mater. 123 (2016) 581–593, https://doi.org/10.1016/j.conbuildmat.2016.07.043.
[23] R. Cornelis, H. Priyosulistyo, I. Satyarno, Workability and Strength Properties of Class C Fly Ash-Based Geopolymer Mortar, vol. 9, 2019.
[24] A.R. Kotwal, Y.J. Kim, J. Hu, V. Sriraman, Characterization and early age physical properties of ambient cured geopolymer mortar based on class C fly ash, Int. J. Concr. Struct. Mater. 9 (1) (2015) 35–43, https://doi.org/10.1007/s40069-014-0085-0.
[25] M. Ibrahim, M.A. Megat Johari, M.K. Rahman, M. Maslehuddin, Effect of alkaline activators and binder content on the properties of natural pozzolan-based alkali activated concrete, Construct. Build. Mater. 147 (2017) 648–660, https://doi.org/10.1016/j.conbuildmat.2017.04.163.
[26] A.A. Adam, Horianto, The effect of temperature and duration of curing on the strength of fly ash based geopolymer mortar, Procedia Eng. 95 (December 2014) (2014) 410–414, https://doi.org/10.1016/j.proeng.2014.12.199.
[27] S. İpek, Macro and micro characteristics of eco-friendly fly ash-based geopolymer composites made of different types of recycled sand, J. Build. Eng. 52 (December 2021) (2022), https://doi.org/10.1016/j.jobe.2022.104431.
[28] N.K. Lee, H.K. Lee, Setting and mechanical properties of alkali-activated fly ash/slag concrete manufactured at room temperature, Construct. Build. Mater. 47 (2013) 1201–1209, https://doi.org/10.1016/j.conbuildmat.2013.05.107.
[29] E. Bachtiar, et al., Correlation of NaOH composition and alkali modulus to compressive strength on geopolymers mortar, ARPN J. Eng. Appl. Sci. 15 (5) (2020) 601–606.
[30] H.E. Elyamany, A.E.M. Abd Elmoaty, A.M. Elshaboury, Setting time and 7-day strength of geopolymer mortar with various binders, Construct. Build. Mater. 187 (2018) 974–983, https://doi.org/10.1016/j.conbuildmat.2018.08.025.
[31] N. Nikoloutsopoulos, A. Sotiropoulou, G. Kakali, S. Tsivilis, Physical and mechanical properties of fly ash based geopolymer concrete compared to conventional concrete, Buildings 11 (5) (2021) 1–14, https://doi.org/10.3390/buildings11050178.
[32] A. Noushini, F. Aslani, A. Castel, R.I. Gilbert, B. Uy, S. Foster, Compressive stress-strain model for low-calcium fly ash-based geopolymer and heat-cured Portland cement concrete, Cem. Concr. Compos. 73 (2016) 136–146, https://doi.org/10.1016/j.cemconcomp.2016.07.004.
[33] P. Nath, P.K. Sarker, Flexural strength and elastic modulus of ambient-cured blended low-calcium fly ash geopolymer concrete, Construct. Build. Mater. 130 (2017) 22–31, https://doi.org/10.1016/j.conbuildmat.2016.11.034.
[34] P.L. Domone, A review of the hardened mechanical properties of self-compacting concrete, Cem. Concr. Compos. 29 (1) (2007) 1–12, https://doi.org/10.1016/j.cemconcomp.2006.07.010.
[35] S.K. Rahman, R. Al-Ameri, A newly developed self-compacting geopolymer concrete under ambient condition, Construct. Build. Mater. 267 (2021), https://doi.org/10.1016/j.conbuildmat.2020.121822.
[36] M.T. Ghafoor, C. Fujiyama, Constitutive model for self-compacting geopolymer mortar based on fly ash content, J. Build. Eng. 71 (March) (2023), 106462, https://doi.org/10.1016/j.jobe.2023.106462.
[37] I. Faridmehr, M.L. Nehdi, G.F. Huseien, M.H. Baghban, A.R.M. Sam, H.A. Algaifi, Experimental and informational modeling study of sustainable self-compacting geopolymer concrete, Sustain. Times 13 (13) (2021), https://doi.org/10.3390/su13137444.
[38] Y.J. Patel, N. Shah, Development of self-compacting geopolymer concrete as a sustainable construction material, Sustain. Environ. Res. 28 (6) (2018) 412–421, https://doi.org/10.1016/j.serj.2018.08.004.
[39] M.E. Gülşan, R. Alzeebaree, A.A. Rasheed, A. Niş, A.E. Kurtoğlu, Development of fly ash/slag based self-compacting geopolymer concrete using nano-silica and steel fiber, Construct. Build. Mater. 211 (2019) 271–283, https://doi.org/10.1016/j.conbuildmat.2019.03.228.
[40] G. Saini, U. Vattipalli, Assessing properties of alkali activated GGBS based self-compacting geopolymer concrete using nano-silica, Case Stud. Constr. Mater. 12 (2020), e00352, https://doi.org/10.1016/j.cscm.2020.e00352.
[41] M.T. Ghafoor, C. Fujiyama, K. Maekawa, Hardened mechanical properties of self compacting geopolymer mortar, J. Adv. Concr. Technol. 20 (4) (2022) 287–299, https://doi.org/10.3151/jact.20.287.
[42] M.T. Ghafoor, C. Fujiyama, November, Performance of Superplasticizers in Alkaline Environment of Self Com- Pacting Geopolymer Mortar, vol. 20, 2022, pp. 676–690, https://doi.org/10.3151/jact.20.676.
[43] ASTM C 618, Standard Specification for Coal Fly Ash and Raw or Calcined Natural Pozzolan for Use in Concrete, ASTM International, West Conshohocken, PA, 2014, https://doi.org/10.1520/C0618, 2012.
[44] M. Nodehi, F. Aguayo, Ultra high performance and high strength geopolymer concrete, J. Build. Pathol. Rehab. 6 (1) (2021) 1–29, https://doi.org/10.1007/s41024-021-00130-5.
[45] EFNARC, The European guidelines for self-compacting concrete, Eur. Guidel. Self Compact. Concr. (May) (2005) 63 [Online]. Available: http://www.efnarc.org/pdf/SCCGuidelinesMay2005.pdf.
[46] Astm, C138, "Standard Test Method for Density (Unit Weight), Yield, and Air Content (Gravimetric),", i, ASTM Int., 2013, pp. 23–26.
[47] C.C. Test, T. Drilled, C.C. Test, B. Statements, ASTM C 39/C 39M – 01, Standard Test Method for Compressive Strength of Cylindrical Concrete Specimens (2014) 3–9, https://doi.org/10.1520/C0039.
[48] ASTM C469-02, Standard Test Method for Static Modulus of Elasticity and Poisson's Ratio of Concrete in Compression, vol. 4, ASTM Stand. B., 2002, pp. 1–5 [Online]. Available: http://portales.puj.edu.co/wjfajardo/mecanica de solidos/laboratorios/astm/C469.pdf.
[49] M.F.M. Tahir, et al., Mechanical and durability analysis of fly ash based geopolymer with various compositions for rigid pavement applications, Materials 15 (10) (2022) 3458, https://doi.org/10.3390/ma15103458.
[50] P. Aggarwal, R. Siddique, Y. Aggarwal, S.M. Gupta, Self-compacting concrete - procedure for mix design, Leonardo Electron. J. Pract. Technol. 7 (12) (2008) 15–24.
[51] G. Sua-Iam, N. Makul, Utilization of limestone powder to improve the properties of self-compacting concrete incorporating high volumes of untreated rice husk ash as fine aggregate, Construct. Build. Mater. 38 (2013) 455–464, https://doi.org/10.1016/j.conbuildmat.2012.08.016.
[52] F. Lolli, J.J. Thomas, K.E. Kurtis, F. Cucinotta, E. Masoero, Early age volume changes in metakaolin geopolymers: insights from molecular simulations and experiments, Cement Concr. Res. 144 (January) (2021), 106428, https://doi.org/10.1016/j.cemconres.2021.106428.
[53] S. Kumaravel, Development of various curing effect of nominal strength Geopolymer concrete, J. Eng. Sci. Technol. Rev. 7 (1) (2014) 116–119, https://doi.org/10.25103/jestr.071.19.
[54] A. Albidah, M. Alghannam, H. Abbas, T. Almusallam, Y. Al-Salloum, Characteristics of metakaolin-based geopolymer concrete for different mix design parameters, J. Mater. Res. Technol. 10 (2021) 84–98, https://doi.org/10.1016/j.jmrt.2020.11.104.
[55] *ACI 318S-14) and Commentary (ACI 318SR-14)*, ACI-318M-14, *Building Code Requirements For Structural Concrete*, 2014.
[56] N.H.A. Shukor Lim, et al., Effect of curing conditions on compressive strength of FA-POFA-based geopolymer mortar, IOP Conf. Ser. Mater. Sci. Eng. 431 (9) (2018), https://doi.org/10.1088/1757-899X/431/9/092007.
[57] E. Muthu Kumar, K. Ramamurthy, Influence of production on the strength, density and water absorption of aerated geopolymer paste and mortar using Class F fly ash, Construct. Build. Mater. 156 (2017) 1137–1149, https://doi.org/10.1016/j.conbuildmat.2017.08.153.
[58] G.F. Huseien, J. Mirza, M. Ismail, M.W. Hussin, Influence of different curing temperatures and alkali activators on properties of GBFS geopolymer mortars containing fly ash and palm-oil fuel ash, Construct. Build. Mater. 125 (2016) 1229–1240, https://doi.org/10.1016/j.conbuildmat.2016.08.153.
[59] H. Zhao, W. Sun, X. Wu, B. Gao, The effect of coarse aggregate gradation on the properties of self-compacting concrete, Mater. Des. 40 (2012) 109–116, https://doi.org/10.1016/j.matdes.2012.03.035.
[60] P. Sajan, T. Jiang, C.K. Lau, G. Tan, K. Ng, Combined effect of curing temperature, curing period and alkaline concentration on the mechanical properties of fly ash-based geopolymer, Clean. Mater. 1 (May) (2021), 100002, https://doi.org/10.1016/j.clema.2021.100002.

[61] M. Triwulan, J.J. Ekaputri, N.F. Priyanka, The effect of temperature curing on geopolymer concrete, MATEC Web Conf. 97 (2017), https://doi.org/10.1051/matecconf/20179701005, 0–5.
[62] M. Khandelwal, P.G. Ranjith, Z. Pan, J.G. Sanjayan, Effect of strain rate on strength properties of low-calcium fly-ash-based geopolymer mortar under dry condition, Arabian J. Geosci. 6 (7) (2013) 2383–2389, https://doi.org/10.1007/s12517-011-0507-0.
[63] B. Kanagaraj, E. Lubloy, N. Anand, V. Hlavicka, T. Kiran, Investigation of physical, chemical, mechanical, and microstructural properties of cement-less concrete – state-of-the-art review, Construct. Build. Mater. 365 (November 2021) (2023), 130020, https://doi.org/10.1016/j.conbuildmat.2022.130020.